25th ABCM International Congress of Mechanical Engineering
October 20-25, 2019, Uberlândia, MG, Brazil

COB-2019-0108
PLANAR 5R SYMMETRICAL PARALLEL MECHANISM SUBJECTED TO CLEARANCES

Fabian Andres Lara-Molina
Edson Hideki Koroishi
Alexandre da Cruz Policarpo
Federal University of Technology - Paraná, Mechanical Engineering Department, Av. Alberto Carazzai 1640, Cornélio Procópio-PR, Brazil.
fabianmolina@utfpr.edu.br,edsonh@utfpr.edu.br

Valder Steffen Jr
LMEst - Structural Mechanics Laboratory, Federal University of Uberlândia, School of Mechanical Engineering, Av. João Naves de Ávila, 2121, Uberlândia, MG, 38408-196, Brazil.
vsteffen@ufu.br

Abstract. *Clearances on the active and passive joints of parallel mechanisms degrade their kinematic positioning accuracy. Therefore, this paper presents a novel methodology to analyze uncertainty effects on the kinematic performance of the parallel mechanism. This contribution aims at analyzing the effect of clearances on the kinematics of the 5R symmetrical parallel mechanism by using numerical simulation. Initially, the complete kinematic model of the mechanism is formulated by considering the clearances with uncertainties that are modeled as random variables. The forward kinematic with the clearances and uncertainties are computed by using the Monte Carlo Method. Finally, the kinematic accuracy is evaluated for several poses within the workspace by considering different link lengths of the mechanism.*

Keywords: *Parallel Mechanism, Kinematics, Uncertainties, Random Variables, clearances*

1. INTRODUCTION

Joints are subject to clearances or position errors that deteriorate the overall performance of the parallel mechanism. Moreover, manufacturing errors and assembling tolerances introduce small variations in the geometry of the links that also produce position errors affecting the performance of the system. Therefore, it is necessary to quantify the effect of these uncertainties in the kinematic performance of the parallel mechanism, i.e., to analyze how these uncertainties affect the performance of parallel mechanism.

The influence of the clearances size and friction coefficient on the dynamic response of planar multi-body system is numerically analyzed (Flores *et al.*, 2006, 2007). Finally, an optimization method for the dynamic design of planar mechanism with clearances at joints has been studied (Feng *et al.*, 2002).The kinematics and workspace of parallel mechanisms have been extensively studied (Merlet, 2006). Specifically, the 5R parallel mechanism has been studied considering the following points: workspace (Liu *et al.*, 2000), singularities (Cervantes-Sánchez *et al.*, 2001) and performance atlases (Gao *et al.*, 1998). On the other hand, uncertain analysis theory has been applied to parallel machines. Jokiel *et al.* (2001) used uncertainty propagation in the calibration of parallel kinematic machines. Chen *et al.* (2013) studied the planar parallel manipulators considering input uncertainties and joint clearance based on the theory of the envelope. Altuzarra *et al.* (2011) present a methodology for analyzing the location of the discontinuities produced by clearances within a 5R planar parallel mechanism. Hu and Li (2011) performed the optimal design of parallel machines under uncertainties. Lara-Molina *et al.* (2016) presented a case study about the forward/inverse kinematics of 5R symmetrical mechanism by considering uncertainties in the link lengths and position error of active joints. Furthermore, Erkaya (2012) has studied the effects of joint clearance on welding robot manipulators in order to analyze the degradation of kinematic and dynamic performance. Therefore, this paper presents a novel methodology to analyze uncertainty effects on the kinematic performance of the parallel mechanism.

This paper aims at analyzing the kinematics of the 5R parallel mechanism subjected to uncertain link lengths, uncertain position error of the active joints and uncertainties in the clearances. In accordance with that, the forward/inverse kinematic model and the workspace were formulated as a function of the aforementioned uncertain parameters by considering the clearances of active and passive joints. The uncertain parameters are modeled as random variables, which are introduced in the kinematic model of the mechanism. The Monte Carlo simulation is used as a stochastic solver to

compute the numerical response of the kinematic model with the uncertain parameters. Finally, the numerical results are analyzed.

2. PLANAR 5R SYMMETRICAL PARALLEL MECHANISM

The 5R symmetrical planar parallel mechanism has two identical kinematic chains. Each kinematic chain has an active or actuated joint, one passive joint and two links. The geometry of the 5R symmetrical parallel mechanism is defined according to Fig. 1(a). The active joints are located at the point A_i and their angular position are defined as θ_i (for $i = 1, 2$). The passive joints are located at the end of each link of the active joints B_i. The end-effector of the mechanism is located at the point P that is defined by the x and y Cartesian coordinates. Additionally, the fixed reference frame O is defined at the midpoint of A_1A_2, therefore the symmetry of the mechanism is defined by $OA_1 = OA_2$, $A_1B_1 = A_2B_2$ and $B_1P = B_2P$. The geometry of the 5R symmetrical mechanism can be completely defined by $OA_i = \overline{r}_3(r_3)$, $A_iB_i = \overline{r}_1(r_1)$ and $B_iP = \overline{r}_2(r_2)$.

For the symmetrical parallel mechanism, the link lengths are stated by $\overline{r}_1$, $\overline{r}_2$ and $\overline{r}_3$ (see Fig. 1(a)). The link lengths can be specified between zero and infinite. Nevertheless, the link length are non-dimensionalized in order to set a normalized value for link lengths; this concept was perviously defined by Gao *et al.* (2001). In accordance with that, it is defined that $D = (\overline{r}_1 + \overline{r}_2 + \overline{r}_3)/3$, thus, the three non-dimensional parameters (r_i, for $i = 1, 2, 3$) are defined by:

$$r_1 = \overline{r}_1/D \qquad r_2 = \overline{r}_2/D \qquad r_3 = \overline{r}_3/D \tag{1}$$

Therefore:

$$r_1 + r_2 + r_3 = 3 \tag{2}$$

Moreover, the end-effector coordinates are also non-dimensionalized as follows:

$$x = \overline{x}/D \qquad y = \overline{y}/D \tag{3}$$

Additionally, the clearances are considered in the active joints, A_i, and the passive joints, B_i and P. These clearances introduce additional degrees of freedom in the geometric model, according to Figs. 1(a) and 1(b). Each clearance in the active joint adds three degrees of freedom: horizontal and vertical displacements (Δx_{A_i} and Δy_{A_i}) and one rotation dhi. Furthermore, each clearance in the passive joint adds two degrees of freedom: two displacements, horizontal and vertical (Δx_{B_i} and Δy_{B_i}).

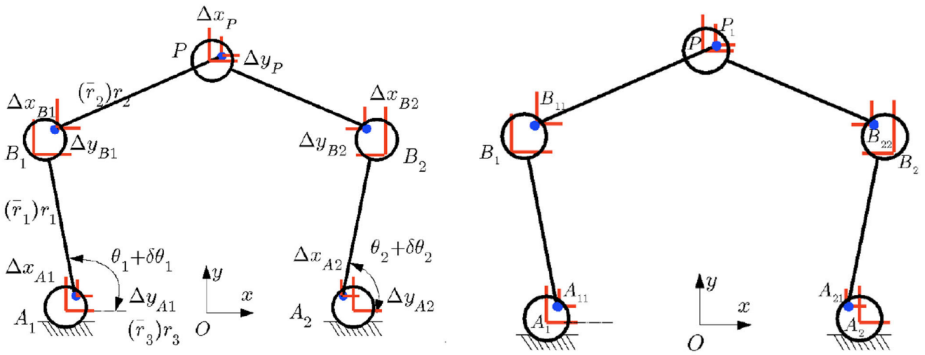

(a) 5R Mechanism. (b) System References.

Figure 1. The 5R symmetrical parallel mechanism.

2.1 The Design Space

The kinematic performance of a parallel mechanism depends on the pose of the end-effector and the dimensions of the links. By considering only the dimensions of the links, each link can vary between zero and infinite. Therefore, the kinematic performance is determined by the links lengths. The design space aims at establishing a determined plot as a function of all link lengths. Therefore, the design space permits to assess all the possible combinations of the links dimensions to compute their correspondent performance indices Liu *et al.* (2006b).

Theoretically, $0 < r_i < 3$ for $i = 1, 2, 3$, nevertheless, some constraints are defined for each parameter:

$$0 < r_1, r_2 < 3 \qquad \text{and} \qquad 0 \leq r_3 \leq 1.5 \tag{4}$$

Based on the Eq. (2) and the constraints of Eq. (4), the design space is defined as a trapezoid shown in Fig. 2(a). Additionally, a planar configuration is also defined based on two orthogonal coordinates s and t (see Fig. 2(b)), thus:

$$s = 2r_1/\sqrt{3} + r_3/\sqrt{3} \tag{5}$$

$$t = r_3 \tag{6}$$

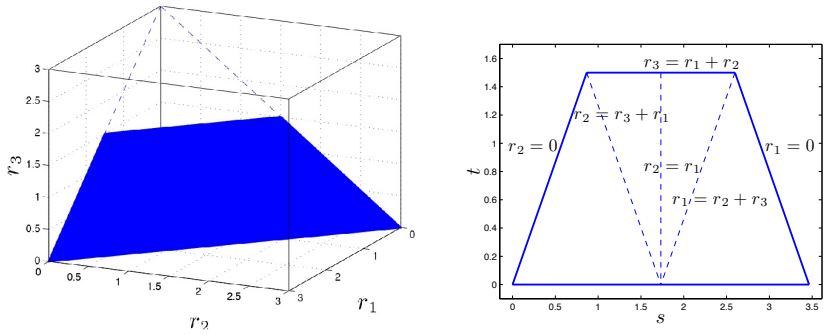

(a) (b)

Figure 2. Design space of the 5R symmetrical mechanism.

The design space can be split in several sub-regions, as presented in Fig. 2(b); these subregions are contoured by lines where r_1, r_2 and r_3 assume given values. Then, r_2 is equal to zero at the left contour of the trapezoid, $r_3 = r_1 + r_2$ at the top, $r_1 = r_2$ in the middle and $r_2 = r_3 + r_1$ on the left dotted line. Consequently, the design space can be analyzed with the help of the aforementioned lines.

2.2 Uncertain Parameters Modeling

The uncertainties in parallel mechanisms are associated with the assembling and manufacturing tolerances and the errors of the actuators Chen *et al.* (2013). These uncertainties consist in small variations around the nominal parameters that produce a variation in the kinematic model performance.

In the present contribution, the uncertainties are introduced in the geometric parameters that affect the kinematic performance of the mechanism: the links length r_i and joints errors of the active joints $\delta\theta_j$, for $j = 1, 2$. The uncertain parameters are modeled as random variables since this formalism allows modeling small deviations around a nominal value. The uncertainties in the link length is defined as follows:

$$\bar{r}_i(\Omega) = \bar{r}_i + \bar{r}_i \delta_r \xi(\Omega) \tag{7}$$

where $\bar{r}_i$ is the nominal link length, δ_r is the maximum percentual deviation around the nominal link length and $\xi(\Omega)$ is the unit normal random variable with mean and variance being zero and one, respectively and Ω is a random process. The unit normal random variable is governed by a normal distribution; this distribution was selected in order to evaluate the uncertain parameters. Additionally, the uncertain link lengths are non-dimensionalized according to $D(\Omega) = (\bar{r}_1(\Omega) + \bar{r}_2(\Omega) + \bar{r}_3(\Omega))/3$. Consequently, the non-dimensional link lengths with uncertainties are defined by: $r_i(\Omega) = \bar{r}_i(\Omega)/D(\Omega)$ for $i = 1, 2, 3$.

On the other hand, the uncertainties in the error of active joints are defined as:

$$\delta\theta_j(\Omega) = \delta_{\theta j} \xi(\Omega) \tag{8}$$

where, $\delta_{\theta j}$ (for $j = 1, 2$) is the maximum dispersion of the joint error and $\xi(\Omega)$ is the unit random variable previously defined in Eq. (7).

The parameters that define the uncertain link lengths and joint errors were determined based on contributions that have experimentally studied uncertainties in the parallel mechanism. The combined effects produced by strut flexibility and thermal effects introduce uncertainties in link lengths of a parallel mechanism. Consequently, the maximum dispersion of these uncertainties was quantified as 0.004% of the link length as stated by Jokiel *et al.* (2001). In addition, position control mismatch and position sensor resolution introduce joint errors in the active joints. The uncertain parameters are defined in table 1.

In the definition of uncertain link length and according to Eq. (1), $D = 1$ by selecting $\bar{r}_i = r_i$. Nevertheless, different link lengths can be considered in order to evaluate a several sizes of the mechanism.

The so-called Monte Carlo method combined with the Latin Hypercube sampling Florian (1992) is used to simulate the kinematics of the mechanism with the considered random uncertainties. The Monte Carlo method combined with the Latin Hypercube permits to evaluate the uncertain response by demanding less computational effort than using only the Monte Carlo method. Additional details about this method can be found at Florian (1992).

Table 1. Parameters of uncertain link lengths and joint errors.

Parameter	$\bar{r}_1(\Omega)$	$\bar{r}_2(\Omega)$	$\bar{r}_3(\Omega)$	$\delta\theta_1(\Omega)$	$\delta\theta_2(\Omega)$
$\bar{r}_i$	r_1	r_2	r_3	-	-
δ_r	0.004%	0.004%	0.004%	-	-
δ_θ [^{o}]	-	-	-	0.05	0.05

2.3 Forward Kinematics

The forward kinematic model sets the position of the end-effector located at the point P as a function of the active joints θ_i. Additionally, the joint errors are also considered. The forward kinematics is solved with the aids of the constraint equation $|\mathbf{b}_i\mathbf{p}| = r_2$, therefore:

$$(x - r_1(\Omega)\cos(\theta_1 + \delta\theta_1(\Omega)) - r_3(\Omega))^2 + (y - r_1(\Omega)\sin(\theta_1 + \delta\theta_1(\Omega)))^2 = r_2(\Omega)^2 \tag{9}$$

$$(x - r_1(\Omega)\cos(\theta_2 + \delta\theta_2(\Omega)) + r_3(\Omega))^2 + (y - r_1(\Omega)\sin(\theta_2 + \delta\theta_2(\Omega)))^2 = r_2(\Omega)^2 \tag{10}$$

From Eqs. (9) and (10) one obtaines:

$$\begin{aligned} x^2 + y^2 - 2(r_1(\Omega)\cos(\theta_1 + \delta\theta_1(\Omega)) - r_3(\Omega))x - 2r_1(\Omega)\sin(\theta_1 + \delta\theta_1(\Omega))y - \ldots \\ 2r_1(\Omega)r_3(\Omega)\cos(\theta_1 + \delta\theta_1(\Omega)) + r_3(\Omega)^2 + r_1(\Omega)^2 - r_2(\Omega)^2 = 0 \end{aligned} \tag{11}$$

$$\begin{aligned} x^2 + y^2 - 2(r_1(\Omega)\cos(\theta_2 + \delta\theta_2(\Omega)) + r_3(\Omega))x - 2r_1(\Omega)\sin(\theta_2 + \delta\theta_2(\Omega))y + \ldots \\ 2r_1(\Omega)r_3(\Omega)\cos(\theta_2 + \delta\theta_2(\Omega)) + r_3(\Omega)^2 + r_1(\Omega)^2 - r_2(\Omega)^2 = 0 \end{aligned} \tag{12}$$

From Eqs. (11) and (12) results:

$$x = ey + f \tag{13}$$

with:

$$\begin{aligned} e =& \frac{r_1(\Omega)(\cos(\theta_1 + \delta\theta_1(\Omega)) - \sin(\theta_1 + \delta\theta_2(\Omega)))}{2r_3(\Omega) + r_1(\Omega)\cos(\theta_2 + \delta\theta_2(\Omega)) - r_1(\Omega)\cos(\theta_1 + \delta\theta_1(\Omega))} \\ f =& \frac{r_1(\Omega)r_3(\Omega)(\cos(\theta_1 + \delta\theta_1(\Omega)) + \cos(\theta_2 + \delta\theta_2(\Omega)))}{2r_3(\Omega) + r_1(\Omega)\cos(\theta_2 + \delta\theta_2(\Omega)) - r_1(\Omega)\cos(\theta_1 + \delta\theta_1(\Omega))} \end{aligned}$$

By substituting Eq. (13) to Eq. (11) results:

$$dy^2 + gy + h = 0 \tag{14}$$

with

$$\begin{aligned} d =& 1 + e^2 \\ g =& 2(ef - er_1(\Omega)\cos(\theta_1 + \delta\theta_1(\Omega)) + er_3(\Omega) - r_1(\Omega)\sin(\theta_1 + \delta\theta_1(\Omega))) \\ h =& f^2 - 2f(r_1(\Omega)\cos(\theta_1 + \delta\theta_1(\Omega)) - r_3(\Omega)) - 2r_1(\Omega)r_3(\Omega)\cos(\theta_1 + \delta\theta_1(\Omega)) \\ & + r_3(\Omega)^2 + r_1(\Omega)^2 - r_2(\Omega)^2 \end{aligned}$$

Considering Eq. (14), y can be obtained as:

$$y = \frac{-g + \sigma\sqrt{g^2 - 4dh}}{2d} \tag{15}$$

From Eq. (15), it is noted that the forward kinematic has two solutions corresponding to $\sigma = 1$ or $\sigma = -1$. In this contribution, $\sigma = 1$ is adopted.

2.4 Workspace of the Mechanism

The region of the workspace that is encompassed by the end-effector when the active joints θ_i vary from 0 to 2π is defined as the theoretical workspace. According to this definition, the collision between the links and the singularities are not considered. The theoretical workspace is enveloped by two the following circles for the first kinematic chain:

$$C_{1o} : (x + r_3(\Omega))^2 + y^2 = (r_1(\Omega) + r_2(\Omega))^2 \tag{16}$$

$$C_{1i} : (x + r_3(\Omega))^2 + y^2 = (r_1(\Omega) - r_2(\Omega))^2 \tag{17}$$

For the second kinematic chain, the workspace is enveloped by the circles:

$$C_{2o} : (x - r_3(\Omega))^2 + y^2 = (r_1(\Omega) + r_2(\Omega))^2 \tag{18}$$

$$C_{2i} : (x - r_3(\Omega))^2 + y^2 = (r_1(\Omega) - r_2(\Omega))^2 \tag{19}$$

The theoretical workspace is defined by the intersection of the circles represented by the Eqs. (16), (17), (18) and (19). The usable workspace is specified as the maximum continuous region inscribed in the theoretical workspace that contains no singular loci inside. Consequently, the usable workspace is bounded by the singular loci outside. Moreover, the *Maximum Inscribed Circle* (MIC) is an index useful to evaluate the flatness of the usable workspace; the MIC is inscribed within the usable workspace and it is tangent to the singular loci Liu *et al.* (2006a). Therefore, the *Maximum Inscribed Workspace* (MIW) is defined as the workspace bounded by the MIC. The MIC is defined as follows:

$$x^2 + (y - y_{MIC})^2 = r_{MIC}^2 \tag{20}$$

where r_{MIC} is the radius and $(0, y_{MIC})$ is the center of the MIC. For the cases corresponding to $r_1(\Omega)+r_3(\Omega) < r_2(\Omega)$, the MIC is defined by:

$$\begin{aligned} r_{MIC} &= (r_1(\Omega) + r_2(\Omega) - |r_1(\Omega) - r_2(\Omega)|)/2 \qquad \text{and} \\ y_{MIC} &= \sqrt{(r_1(\Omega) + r_2(\Omega) + |r_1(\Omega) - r_2(\Omega)|)^2/4 - r_3(\Omega)^2} \end{aligned} \tag{21}$$

For the cases corresponding to $r_1(\Omega) + r_3(\Omega) > r_2(\Omega)$, the radius and the center of the MIC are defined by:

$$\begin{aligned} r_{MIC} &= |y_{MIC}| - y_{col} \qquad \text{and} \\ y_{MIC} &= \frac{(r_1(\Omega) + r_2(\Omega) + y_{col})^2 - r_3(\Omega)^2}{2(r_1(\Omega) + r_2(\Omega) + y_{col})} \end{aligned} \tag{22}$$

with $y_{col} = \sqrt{r_1(\Omega)^2 - (r_2(\Omega) - r_3(\Omega))^2}$.

The workspace of the mechanism is illustrated in Fig. 3 according to the formulation previously presented by considering the nominal parameters without uncertainties: r_1=1.2, r_2=1.0, r_3=0.8 without uncertainties.

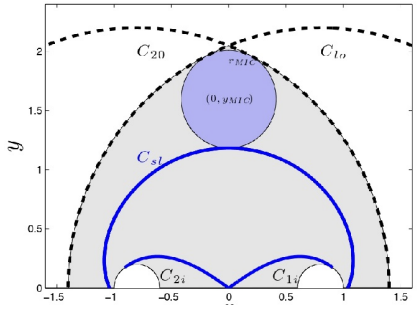

Figure 3. Workspace: usable workspace, MIW and singular loci.

2.5 Clearances

The clearances are considered in the active (see Fig. 4(a)) and the passive joints (see Fig. 4(b), 4(c)). Each active joint introduces three additional degrees of freedom: Δx_{A_i}, Δy_{A_i} associated to the radial clearance between the journal and the bearing and dhi produced by the angular position error of the motor. Furthermore, each passive joint introduces two additional degrees of freedom by the radial clearance: Δx_{B_i}, Δy_{B_i}. Several assumptions are considered to include the additional degrees of freedom (Δx_{A_i}, Δy_{A_i}, Δx_{B_i}, Δy_{B_i}, $\delta\theta_i$, Δx_P, Δy_P) of the clearances into the kinematic model of the parallel mechanism. These assumptions are described as follows:

1. The radial clearance of all clearances are equal, and they are defined by r_c.

2. The bearing is always in contact with the journal according to the motion type defined by Erkaya (2012); this allows evaluating the maximum effect of the clearances on the position error of the end-effector.

3. The passive joint of the end-effector is in free motion type as defined by Erkaya (2012). Therefore, the imposed values for υ_{A_i} and υ_{B_i} must ensure that $|\mathbf{p}_1\mathbf{p}| < r_c$, to respect the kinematic constaints (see Fig. 2c), with $\mathbf{p}_1 = \begin{bmatrix} x + \Delta x_{B_1} & y + \Delta y_{B_1} \end{bmatrix}^T$ and $\mathbf{p}_2 = \begin{bmatrix} x + \Delta x_{B_2} & y + \Delta y_{B_2} \end{bmatrix}^T$.

4. The clearances are considered for the static case, i.e., the static case where $\Delta\dot{x}_{A_i} = \Delta\dot{y}_{A_i} = \Delta\dot{x}_{B_i} = \Delta\dot{y}_{B_i} = \delta\dot{\theta} = 0$.

5. The links rotate along the journal axis that is perpendicular to the xy plane.

6. The journal does not translate with the bearing, i.e., the displacements of clearance are not propagated within each kinematic chain.

7. The uncertainties are introduced in the angular position of the journals defined by the angles υ_{A_i} and υ_{B_i} and r_c remains constant.

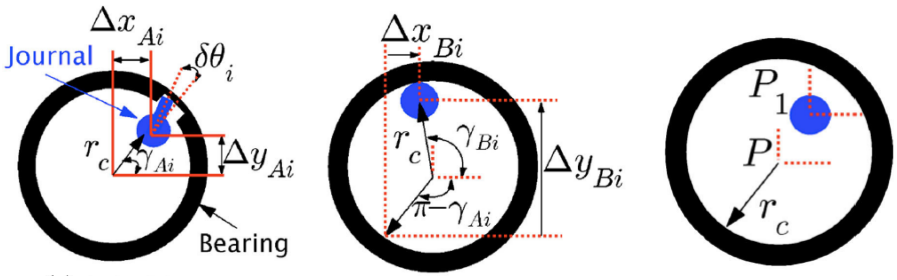

(a) Active Joints. (b) Passive Joints. (c) End-Effector Joint.

Figure 4. Clearances Model: active and passive joints.

The uncertainties in the clearances of active joints are defined by the following expressions based on the previous assumptions:

$$\Delta x_{A_i}(\Omega) = r_c \cos(\upsilon_{A_i}(\Omega)) \qquad \Delta y_{A_i}(\Omega) = r_c \sin(\upsilon_{A_i}(\Omega)) \qquad \delta\theta_i(\Omega) = \delta_{\theta_i}\xi(\Omega) \tag{23}$$

where, $\upsilon_{A_i}(\Omega)$, δ_{θ_i} (for $i = 1, 2$) is the maximum dispersion of the position error of the active joint and $\xi(\Omega)$ is the unit random variable.

Similarly, the uncertainties in the clearances of passive joints are defined by:

$$\begin{aligned} \Delta x_{B_i}(\Omega) &= r_c \begin{bmatrix} \cos(\upsilon_{B_i}(\Omega)) & -\cos(\pi - \upsilon_{A_i}(\Omega)) \end{bmatrix}^T \\ \Delta y_{B_i}(\Omega) &= r_c \begin{bmatrix} \sin(\upsilon_{B_i}(\Omega)) & -\sin(\pi - \upsilon_{A_i}(\Omega)) \end{bmatrix}^T \end{aligned} \tag{24}$$

.

3. KINEMATIC PERFORMANCE ANALYSIS

The kinematic performance analysis consists in analyzing the kinematic accuracy of the mechanism considering the position of the end-effector in several poses within the usable workspace subjected to uncertainties.

Several cases within the design space are selected, i.e, several values for s, and t are considered. Moreover, the corresponding link length r_1, r_2 and r_3 for the considered cases are shown in Table 2.

The kinematic performance analysis includes the analysis of the forward kinematic subjected to uncertainties and the Local Conditioning Index (LCI) over the usable workspace. The forward kinematic subjected to uncertainties was evaluated for several poses within the usable workspace. Specifically, the position of the end-effector was assessed considering the uncertainties through the Monte Carlo simulation. To evaluate comparatively the effect of uncertainties among the different poses, every single pose subjected to uncertainties is inscribed into a circle, centered at the position of end-effector with nominal parameters and non-dimensional radius of 0.005.

Table 2. Cases of analysis within the design space.

Case	s	t	r_1	r_2	r_3
$a)$	2.77	0.08	2.00	0.20	0.80
$b)$	1.00	0.80	0.47	1.73	0.80
$c)$	1.44	1.30	0.60	1.10	1.30
$d)$	1.80	0.25	0.75	2.00	0.25

3.1 Case $a)$

Figure 5(a) shows the different poses where the forward kinematics were evaluated over the usable workspace. In addition, Fig. 5(b) shows the forward kinematics solution for every single pose inscribed in the circle; this result permits to establish a comparative evaluation of the variation in the position of the end-effector produced by the uncertainties.

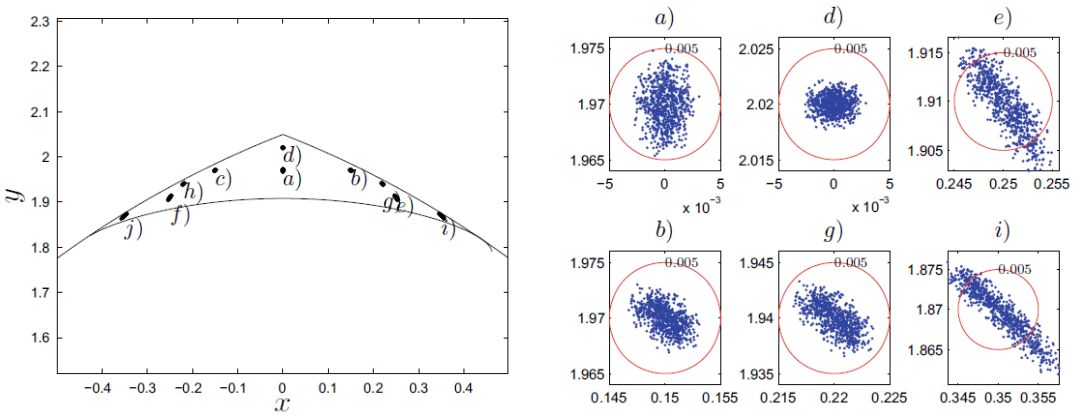

(a) 5R Mechanism. (b) System References.

Figure 5. Forward kinematics for case a: (a) poses over the usable workspace, (b) zoom of poses.

Figure 3. shows the behavior of the LCI over the usable workspace. For this, case one can observe that the LCI suffers a significant variation over the usable workspace. Additionally, as indicated in Fig. 5(b), the most expressive variations in the position of the end-effector are obtained for poses with low LCI. This behavior can be observed specifically, for poses e and i, which are located on the borders of the usable workspace. The characteristics analyzed, in this case, results in an unsatisfactory performance of the mechanism as indicated by the low kinematic dexterity and great influence of the uncertainties on the kinematic positioning of the end-effector.

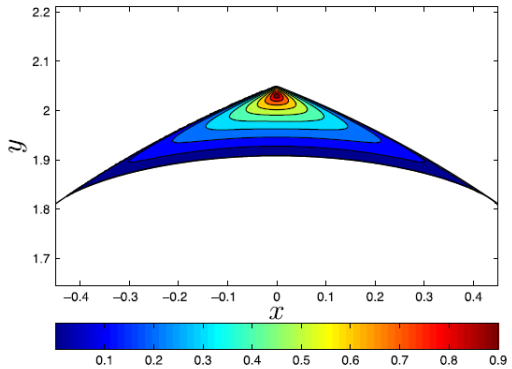

Figure 6. LCI over the usable workspace for case a.

3.2 Case $b)$

Figure 7 shows the position of the end-effector subjected to uncertainties considering the case $b)$ of Table 2. Figure 7(a) shows that the effect of the uncertainties on the position of the end-effector is small for the poses considered, i.e., the

variation of the end-effector position is small. This behavior can be observed for all the poses evaluated in Fig 7(b).

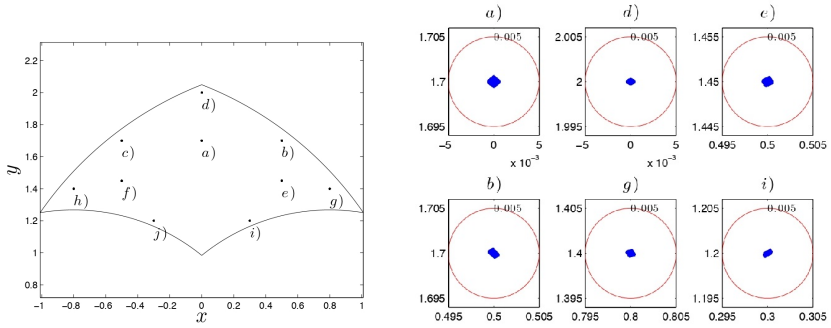

(a) (b)

Figure 7. Forward kinematics for case b): (a) Poses over the usable workspace, (b) Zoom of poses.

As observed in Fig. 8, the LCI has a high value ($LCI = 0.9$); this indicates an isotropic kinematic behavior of the mechanism. Moreover, LCI does not suffer a meaningful variation over the usable workspace, except on the external borders of the workspace. Therefore, the good dexterity performance over the usable workspace contributes to reducing the effects of uncertainties in the kinematic accuracy of the mechanism.

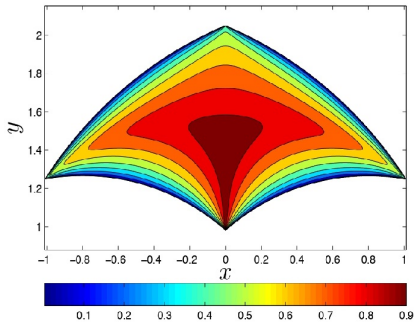

Figure 8. LCI over the usable workspace for case b).

3.3 Case c)

Figure 9 show the position of the end-effector subjected to uncertainties. Figure 9(a) shows that the effect of uncertainties in the position of the end-effector deepens on the considered pose, i.e., the variation of the end-effector position increases for positions close to the borders of the workspace, because of these borders contains singular loci poses. This behavior can be observed for all the poses evaluated in Fig 9(b).

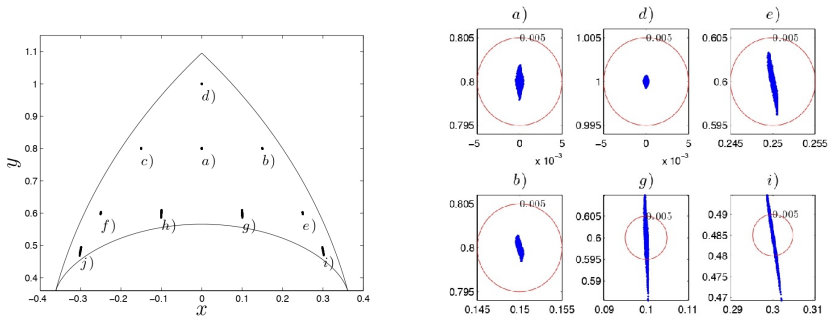

(a) (b)

Figure 9. Forward kinematics for case c): (a) Poses over the usable workspace, (b) Zoom of poses.

Figure 10 shows the LCI over the usable workspace. The most significant variations in the position of the end-effector produced by the uncertainties are obtained for poses with low LCI, which are located in the borders of the workspace for

poses: $e)$, $g)$ and $i)$ (see Fig 9(b)). Furthermore, it is observed that the LCI suffers an important variation over the usable workspace.

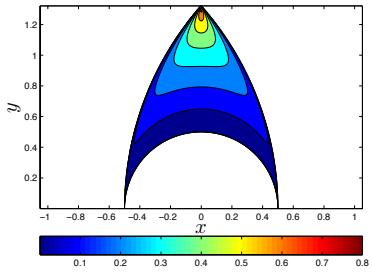

Figure 10. LCI over the usable workspace for case $c)$.

3.4 Case $d)$

The results for case $d)$ are presented in Figs. 11 and 12. The variation in the position of the end-effector is small as compared with the previous cases. For all the cases the end-effector position is inscribed into the circles indicating a low effect of the uncertainties considering this set of link lengths.

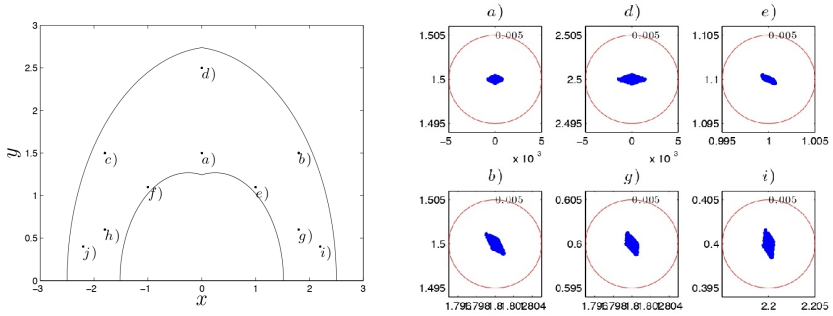

(a) (b)

Figure 11. Forward kinematics for case $d)$: (a) Poses over the usable workspace, (b) Zoom of poses.

Figure 12 shows that LCI attains an intermediate maximum value, where $\max(LCI) = 0.55$. However, LCI has a uniform value over the usable workspace, i.e., LCI does not suffer a significant variation except at the workspace borders. This condition permits to ensure an acceptable kinematic accuracy as it was presented in Fig. 11.

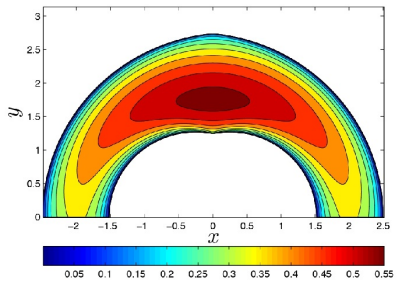

Figure 12. LCI over the usable workspace for case $d)$.

4. CONCLUSIONS

the kinematic performance analysis illustrated the effect of uncertainties in the kinematic positioning of the end-effector of the mechanism for a set of given link lengths. Consequently, the kinematic performance analysis permitted to describe the kinematic performance of the mechanism based on the performance atlases subjected to uncertainties, i.e.,

the behavior of the mechanism can be predicted by examining the performance atlases in a design procedure taking into account the uncertainties in link lengths and joint errors.

Future works will encompass the analysis of the dynamic performance of planar parallel mechanisms considering uncertainties.

5. ACKNOWLEDGEMENTS

The authors express their acknowledgements to the Graduate Program in Mechanical Engineering of the Federal University of Technology - Paraná funded by CAPES. The authors are also thankful for the financial support provided to the present research effort by CNPq (427204/2018-6).

6. REFERENCES

Altuzarra, O., Aginaga, J., Hernández, A. and Zabalza, I., 2011. "Workspace analysis of positioning discontinuities due to clearances in parallel manipulators". *Mechanism and Machine Theory*, Vol. 46, No. 5, pp. 577–592.

Cervantes-Sánchez, J.J., Hernández-Rodríguez, J.C. and Angeles, J., 2001. "On the kinematic design of the 5R planar, symmetric manipulator". *Mechanism and Machine Theory*, Vol. 36, No. 11, pp. 1301–1313.

Chen, G., Wang, H. and Lin, Z., 2013. "A unified approach to the accuracy analysis of planar parallel manipulators both with input uncertainties and joint clearance". *Mechanism and Machine Theory*, Vol. 64, pp. 1–17.

Erkaya, S., 2012. "Investigation of joint clearance effects on welding robot manipulators". *Robotics and Computer-Integrated Manufacturing*, Vol. 28, No. 4, pp. 449–457.

Feng, B., Morita, N. and Torii, T., 2002. "A new optimization method for dynamic design of planar linkage with clearances at joints—optimizing the mass distribution of links to reduce the change of joint forces". *Journal of Mechanical Design*, Vol. 124, No. 1, pp. 68–73.

Flores, P., Ambrósio, J., Claro, J.P. and Lankarani, H., 2007. "Dynamic behaviour of planar rigid multi-body systems including revolute joints with clearance". *Proceedings of the Institution of Mechanical Engineers, Part K: Journal of Multi-body Dynamics*, Vol. 221, No. 2, pp. 161–174.

Flores, P., Ambrósio, J., Claro, J.C.P., Lankarani, H. and Koshy, C., 2006. "A study on dynamics of mechanical systems including joints with clearance and lubrication". *Mechanism and Machine Theory*, Vol. 41, No. 3, pp. 247–261.

Florian, A., 1992. "An efficient sampling scheme: updated latin hypercube sampling". *Probabilistic engineering mechanics*, Vol. 7, No. 2, pp. 123–130.

Gao, F., Liu, X.J. and Chen, X., 2001. "The relationships between the shapes of the workspaces and the link lengths of 3-dof symmetrical planar parallel manipulators". *Mechanism and Machine Theory*, Vol. 36, No. 2, pp. 205–220.

Gao, F., Liu, X. and Gruver, W.A., 1998. "Performance evaluation of two-degree-of-freedom planar parallel robots". *Mechanism and Machine Theory*, Vol. 33, No. 6, pp. 661–668.

Hu, Y. and Li, B., 2011. "Robust design and analysis of 4PUS–1RPU parallel mechanism for a 5-degree-of-freedom hybrid kinematics machine". *Proceedings of the Institution of Mechanical Engineers, Part B: Journal of Engineering Manufacture*, Vol. 225, No. 5, pp. 685–698.

Jokiel, B., Ziegert, J.C. and Bieg, L., 2001. "Uncertainty propagation in calibration of parallel kinematic machines". *Precision Engineering*, Vol. 25, No. 1, pp. 48–55.

Lara-Molina, F.A., Koroishi, E.H. and Bolzon, V., 2016. "Stochastic analysis of the kinematic performance of a planar 5R symmetrical parallel mechanism." In *Transdisciplinary Engineering: Crossing Boundaries*. Vol. 4 of *Advances in Transdisciplinary Engineering*, pp. 563–572.

Liu, X.J., Wang, J. and Gao, F., 2000. "Performance atlases of the workspace for planar 3-DOF parallel manipulators". *Robotica*, Vol. 18, No. 05, pp. 563–568.

Liu, X.J., Wang, J. and Pritschow, G., 2006a. "Kinematics, singularity and workspace of planar 5R symmetrical parallel mechanisms". *Mechanism and Machine Theory*, Vol. 41, No. 2, pp. 145–169.

Liu, X.J., Wang, J. and Pritschow, G., 2006b. "Performance atlases and optimum design of planar 5R symmetrical parallel mechanisms". *Mechanism and machine theory*, Vol. 41, No. 2, pp. 119–144.

Merlet, J.P., 2006. *Parallel robots*, Vol. 128. Springer Science & Business Media.

7. RESPONSIBILITY NOTICE

The following text, properly adapted to the number of authors, must be included in the last section of the paper:
The author(s) is (are) the only responsible for the printed material included in this paper.